**Title of Publication** *Edited by M.G. Chu, D.A. Granger and Q. Han*
***TMS (The Minerals, Metals & Materials Society), 2004***

# CONDUCTION AND RADIATION PARAMETERS FOR ANALYTICAL MODELS OF DIFFERENTIAL SCANNING CALORIMETRY INSTRUMENTS

Adrian S. Sabau[1], Wallace D. Porter[1], Jay I. Frankel[2]

[1]Oak Ridge National Laboratory; Oak Ridge, TN 37831-6083, USA
[2]Mechanical and Aerospace Engineering and Engineering Science Department;
University of Tennessee; Knoxville, TN 17996, USA

Keywords: Heat Flux Differential Scanning Calorimeter, temperature lag, analytical model

## Abstract

Differential Scanning Calorimetry (DSC) measurements are routinely used to determine enthalpies of phase change, phase transition temperatures, glass transition temperatures, and heat capacities. DSC data has also been used to estimate the fractional latent heat release during phase changes. To date, DSC measurements are plagued by temperature lags due to the fact that the temperatures are measured using thermocouples that are placed at a different location than that of the sample and reference materials.

In this study, the temperature lags, which are inherent to the measurement process, are estimated through a computational analysis of the raw DSC data. An analytical model is presented that accounts for different heat transfer mechanisms among instrument components. Through a direct analysis, it is shown that the proposed analytical model can accurately describe the experimental data. The direct analysis presented is to be complemented by inverse process analysis in order to determine more accurate values for the model parameters.

## Introduction

One of the main barriers in the analysis of materials processing and industrial applications is the lack of accurate experimental data on the material thermophysical properties. To date, the measurement of most high-temperature thermophysical properties is often plagued by temperature lags. These temperature lags are inherent to the measurement arrangement since (a) sample temperature is recorded by using a thermocouple that is placed at a different location than that of the sample, and (b) there is a non-homogeneous temperature distribution within the DSC instrument. By performing a computational analysis of the measurement process, the temperature lags can be estimated and their effect can be taken into account in determining the thermophysical properties.

Gray (1968) proposed one of the first models to describe the heat flow in DTA cells that has been adopted for the study of DSC instruments. This methodology has been used with little change even in more recent studies for determining solid fraction distribution as a function of temperature for commercial alloys (Jeng and Chen, 1997). Wolfinger et al. (2001) showed that the sample emissivity and reference emissivity have to be considered only when the DSC experiments are performed without using lids on crucibles. Dong and Hunt (2001) developed and analytical model for the DSC heat flux instrument by considering that the instrument can be represented by a certain number of regions of uniform temperatures. However, their model includes some heat transfer features that do not exist in the instrument, such as conduction paths

between the sample plates and furnace. Speyer (1993) used simplex algorithms to desmear the raw signal from DTA/DSC peaks. Kempen et al. (2003) modeled the Netzsch DSC 404C heat flux instrument, using the DTA methodology. In their approach, a methodology was proposed for determining model parameters by employing DSC measurements for two known sample materials, one that has a smooth specific heat capacity, *Cp,* and the other one that has a sharp transition. The heat transfer mechanisms are oversimplified, e.g., only the plates and pans are considered in the model and a conduction path between the sample plates and furnace is considered. In order the calibrate the thermocouple, a temperature shift of the thermocouple is introduced, while the temperature lag between the sample and sample plate is not accurately determined since the sample container is assumed to have the same temperature as the sample itself.

Danley (2003) introduced a new DSC sensor design that comprises two differential temperature measurements instead of one and an additional temperature measurement of the large container that supports the plates. In his approach, Danley (2003) improved the traditional DSC models, for the plate and pans, by including additional temperature data measured by the sensing unit. Boettinger and Kattner (2002) presented a DTA model in which each part in the instrument is considered to have a uniform temperature. This approach was enhanced with kinetic models for metallic systems and can be used to analyze DTA signals from unknown multicomponent engineering alloys.

## Typical DSC Experimental Results

The data provided by the DSC heat flux instrument are the voltage difference between the two thermocouples and the temperature of one thermocouple. The voltage difference is proportional to the temperature difference between the thermocouples. After post processing the raw signal according to instrument manufacturer, the heat flow between the sample and reference side of the instrument is obtained (Figure 1a). The data shown in Figure 1a was obtained with a Stanton-Redcroft DSC instrument. By integrating partial areas between the base line and DSC curve, the fractional latent heat release can be determined (Figure 1b). For most alloys, the fractional latent heat released during solidification correlates directly to the fraction solid. Most of the time the data generated cannot be used since large discrepancies are noticed between the values for solidus, eutectic, and liquidus temperature.

The liquidus and solidus temperatures can be determined from the DSC measurements performed during cooling and heating, respectively. Due to the instrument time constant effects, the solidus cannot be determined from DSC conducted on cooling. Thus, the fractional latent heat (or solid fraction), which is determined from DSC on cooling, extends to lower temperatures than the solidus. This data at temperatures near the solidus is very important for the prediction of casting defects such as microporosity and hot tearing, which occurs when low amounts of liquid fraction are still present in the alloy. In order to obtain more accurate data on fraction solid versus temperature, an analysis of the DSC system must be made.

## Components of the DSC Instrument

The Netzsch DSC 404C instrument, with a high accuracy heat capacity sensor, is considered in this study. In Figure 2a, a picture of the sensing unit is shown. The individual components of the DSC sensing system are identified and a schematic of the sensing unit is shown in Figure 2b. Based on the DSC sensing system construction, the following parts were identified: (1) sample plate, (2) reference plate, (3) container, (4) sample container, (5) reference container, (6) alumina disk, and (7) sample. The sensing unit is held by a stem and is placed into a furnace. The furnace inner diameter is very close to that of the alumina disk. Sometimes, a sample of known material (8) is placed in the reference container.

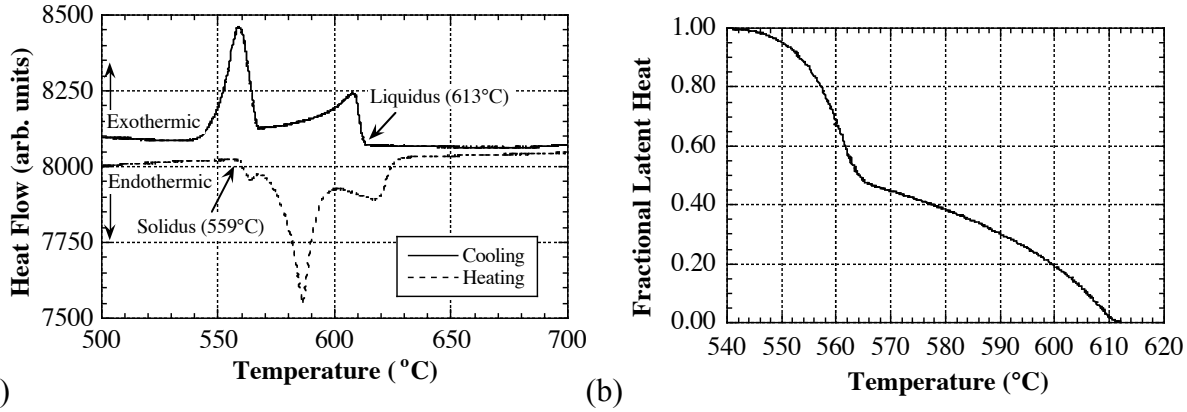


(a) (b)

Figure 1. A356 aluminum alloy (a) DSC data indicating that liquidus, eutectic, and solidus temperatures are 613, 574, and 559 °C, respectively. (b) fractional latent heat determined using DSC at cooling. The fraction latent heat extends to 545 °C, well below the solidus.

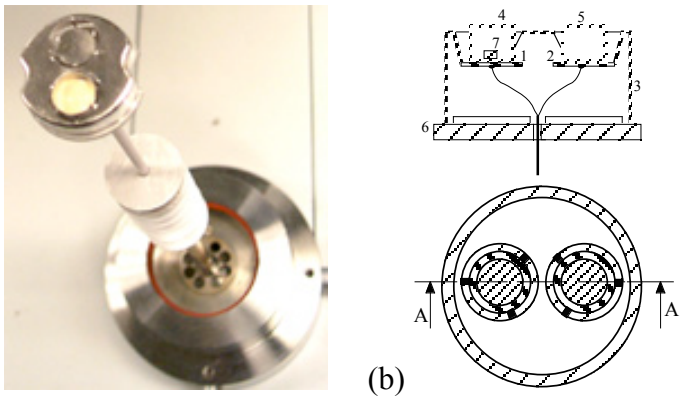


(a) (b)

Figure 2. Cell mounting for typical heat flux type DSC head system used for high-temperature applications: (a) picture and (b) schematic of DSC sensing system.

## Constitutive Equations for the DSC Instrument

A system of nonlinear ordinary differential equations, which accounts for the conduction and radiation heat transfer within the instrument, is presented. Temperatures are normalized with respect to the initial temperature, i.e., $y=T/T_o$. The most complex model, which includes all the heat transfer interactions between different components of the DSC sensing unit, is shown in Table I. The mathematical model is based on the assumption that each component is isothermal and that the heat transfer among components occurs by conduction and radiation. The thermal resistances in the system are represented by effective conduction time constants, $\tau_C$, and radiation time constants, $\tau_R$. An analysis of the model features is presented in later sections with the aim of formulating one of the simplest models that can qualitatively reproduce all the typical features of a DSC signal.

In the Table I, $c_k = C_p^k(y_k)/C_p^k(1)$. $c_{f7} = \tau L_7/C_p^7(1)T_0 + y_m\left(C_p^{7,L} - C_p^{7,S}\right)/C_p^7(1)$, where $L_7$ is the latent heat of the sample material, $C_p^{7,L}$ is the specific heat of the liquid metal at the melting point, $C_p^{7,S}$ is the specific heat of the pure metal in the solid state at the melting point. For pure metal or eutectic alloys, the phase change occurs at a single temperature, $T_m$, and $y_m = T_m/T_0$. During the phase change, the sample temperature is considered constant while its solid fraction varies according to the energy balance within that time step. Since the controller thermocouple is located away from the furnace walls, a temperature lag between the controller temperature and furnace wall temperature was considered.

Table I. Analytical model of the DSC instrument.

| DSC assembly part | dimensionless variable | equation |
|---|---|---|
| furnace | $y_0$ | $\frac{dy_0}{dt} = \frac{y_P - y_0}{\tau_{CF}}$ |
| reference plate | $y_1$ | $c_1 \frac{dy_1}{dt} = \frac{y_3 - y_1}{\tau_{C1}} + \frac{y_3^4 - y_1^4}{\tau_{R1}} + \frac{y_4 - y_1}{\tau_{C3}} + \frac{y_6^4 - y_1^4}{\tau_{R4}}$ |
| sample plate | $y_2$ | $c_2 \frac{dy_2}{dt} = \frac{y_3 - y_2}{\tau_{C2}} + \frac{y_3^4 - y_2^4}{\tau_{R1}} f_1 + \frac{y_5 - y_2}{\tau_{C4}} + \frac{y_6^4 - y_2^4}{\tau_{R4}} f_1$ |
| container | $y_3$ | $c_3 \frac{dy_3}{dt} = \frac{y_1 - y_3}{\tau_{C1}} f_2 + \frac{y_2 - y_3}{\tau_{C2}} \frac{f_2}{f_1} + \frac{y_0^4 - y_3^4}{\tau_{R2}} + \frac{y_6^4 - y_3^4}{\tau_{R5}}$ |
| reference container | $y_4$ | $c_4 \frac{dy_4}{dt} = \frac{y_1 - y_4}{\tau_{C3}} f_3 + \frac{y_0^4 - y_4^4}{\tau_{R3}} + \frac{y_8 - y_4}{\tau_{C5}} f_{10} + \frac{y_5^4 - y_4^4}{\tau_{R8}}$ |
| sample container | $y_5$ | $c_5 \frac{dy_5}{dt} = \frac{y_2 - y_5}{\tau_{C4}} f_4 + \frac{y_0^4 - y_5^4}{\tau_{R3}} f_5 + \frac{y_7 - y_5}{\tau_{C6}} f_8 + \frac{y_4^4 - y_5^4}{\tau_{R8}} f_5$ |
| disk | $y_6$ | $c_6 \frac{dy_6}{dt} = \frac{y_3^4 - y_6^4}{\tau_{R5}} f_6 + \frac{y_0^4 - y_6^4}{\tau_{R6}} f_7 + \frac{y_{sce} - y_6}{\tau_{C7}} + \frac{y_{sce}^4 - y_6^4}{\tau_{R7}}$ |
| sample material | $y_7, f_{S7}$ | $c_7 \frac{dy_7}{dt} + c_{f7} \frac{df_{S7}}{dt} = \frac{y_5 - y_7}{\tau_{C6}} f_9,$ |
| reference material | $y_8$ | $c_8 \frac{dy_8}{dt} = \frac{y_4 - y_8}{\tau_{C5}} f_{11}$ |

The set point temperature is defined as the temperature set by the operator and is usually a linear variation in time given by the constant heating or cooling rate, i.e., $y_P(t) = 1 + \sum_{n=1}^{N} (R_n / T_0)(t - t_n) H(t - t_n)$, where H is the Heaviside function. In the above approach, numerous parameters are required to be determined. In order to describe the system with minimal components, an analysis must be performed in order to ascertain the effect of including each of the components and its associated model parameters. Some of these physical parameters can be determined with the aid of special experiments while others will be determined with the aid of an inverse analysis of parameter-estimation type. The component materials and mass are shown in Table II. Specific scaling parameters are given in Table III.

Based on the scaling used in equations (Table I), the radiation factors can be estimated using the following relationship $\tau_R = mC_p G / \sigma T_0^3$, where $m$ – mass, $Cp$ is the specific heat, $G = (1 - \varepsilon_1)/A_1\varepsilon_1 + (1 - \varepsilon_2)/A_2\varepsilon_2 + 1/A_1 F_{12}$, $\varepsilon$ is the emissivity, A is the component area, $F$ is a view factor, $T_0$=300K, and $\sigma$ is the Stefan Boltzman constant. Thus, order of magnitude estimations for the time constants can be made based on geometry and thermophysical properties of the components. Assuming that $A_1 >> A_2$ and $A_1 = m_1/(t_i \rho_i)$, where $t$ is the component thickness and $\rho$ its density, we obtain that $G\, m_1 = t_1 \rho_1 (1/\varepsilon_1 + 1/F_{12} - 1)$. Using the pure platinum properties and $F_{30}$=1, we obtain that $\tau_{R2} = m_3 C_{Pt} G_{30} / \sigma T_0^3 = 100\, G_{30}$ where $G_{30} = 1/\varepsilon_{Pt} A_3 = t_3 \rho_3 / \varepsilon_{Pt} m_3$. For a container thickness, $t_3$=0.015 cm, platinum density, 21.5g/cm$^3$, platimum emissivity, $\varepsilon_P$=0.1, we obtain a lower estimate of $\tau_{R2} \approx 300$ s. Considering the ratio of specific heats of alumina and platinum materials, $C_A/C_P$=5.8, alumina emissivity, $\varepsilon_A$=0.5, and the thickness ratios $t_1/t_3$=0.7, $t_4/t_3$=3.6, $t_6/t_3$=8.6, the following order of magnitude approximations for time constants associated with radiation effects were obtained (Table IV).

Table II. The material and mass of each component in the DSC system.

| Part | Reference plate ($m_1$) | Sample plate ($m_2$) | Container ($m_3$) | Reference container ($m_4$) | Sample container ($m_5$) | Disk ($m_6$) |
|---|---|---|---|---|---|---|
| Material | Platinum | Platinum | Platinum | *Platinum* | *Platinum* | Alumina |
| Mass [g] | 0.103 | 0.103 | 1.21 | 0.2596 | 0.2558 | 1.53 |

For latent heat measurements, the reference and sample containers are made of alumina and their mass is $m_4$=0.2481 and $m_5$=0.2437 g, respectively.

Table III. Mass factors in the analytical DSC model (f7=f8=f10=1).

| Factor | $f_1$ | $f_2$ | $f_3$ | $f_4$ | $f_5$ |
|---|---|---|---|---|---|
| Expression | *m1/m2* | *m1/m3* | $\frac{m_1 C_p^1(1)}{m_4 C_p^4(1)}$ | $\frac{m_2 C_p^2(1)}{m_5 C_p^5(1)}$ | *m4/m5* |
| Factor | $f_6$ | $f_9$ | $f_{11}$ | | |
| Expression | $\frac{m_3 C_p^3(1)}{m_6 C_p^6(1)}$ | $\frac{m_5 C_p^5(1)}{m_7 C_p^7(1)}$ | $\frac{m_4 C_p^4(1)}{m_8 C_p^8(1)}$ | | |

Table IV. Ratio between time constants associated with radiation effects.

| $\tau_{R1}/\tau_{R2}$ | $\tau_{R3}/\tau_{R2}$ | $\tau_{R4}/\tau_{R2}$ | $\tau_{R5}/\tau_{R2}$ | $\tau_{R6}/\tau_{R2}$ |
|---|---|---|---|---|
| $\frac{m_1}{m_3}\frac{G_{13}}{G_{30}}$ | $\frac{m_4}{m_3}\frac{C_A}{C_P}\frac{G_{40}}{G_{30}}$ | $\frac{m_1}{m_3}\frac{G_{26}}{G_{30}}$ | $\frac{G_{36}}{G_{30}}$ | $\frac{m_6}{m_3}\frac{C_A}{C_P}\frac{G_{60}}{G_{30}}$ |
| $\frac{t_1(1/\tau_P+1/F_{13}\tau_1)}{t_3(1/\tau_P+1/F_{30}\tau_1)}$ | $\frac{C_A t_4 \tau_4(1/\tau_A+1/F_{40}\tau_1)}{C_P t_3 \tau_3(1/\tau_P+1/F_{30}\tau_1)}$ | $\frac{t_1(1/\tau_P+1/F_{16}\tau_1)}{t_3(1/\tau_P+1/F_{30}\tau_1)}$ | $\frac{1/\tau_P+1/F_{36}\tau_1}{1/\tau_P+1/F_{30}\tau_1}$ | $\frac{C_A t_6 \tau_6(1/\tau_A+1/F_{60}\tau_1)}{C_P t_3 \tau_3(1/\tau_P+1/F_{30}\tau_1)}$ |
| 1 | 1 | 0.7 | 1 | 2.4 |

The conduction time constants, between two components that make contact over an area, A, can be defined as a function of interface thermal conductance, $h$, as $\tau_C = m C_p / A h$. Using the properties of pure platinum and the dimensions of the sample plate, A=2x10$^{-5}$ m$^2$ the following estimate can be made for $\tau_{C3}[s] = m_1 C_p^1 / A_1 h_{14} = 650/h_{14}[W/m^2K]$.

## Plate-Container Interaction

It is desirable to determine as many parameters as possible from independent experiments. Based on the structure of the DSC sensing unit, the time constants associated with conduction through the plates and thermocouple can be determined based on simple tests. In order to mimic a step function, a small heated sample was held for a short time on one plate at a time. Since the experiment is conducted at low temperatures, a linear system of three equations has been considered for the empty assembly made up of the reference plate, sample plate, and large container. The analytical solution for this linear system with $m_{SP}/m_C = 0.08 << 1$ yields a signal with two decaying exponentials of the form $a + b\exp(\tau t/\tau) + c\exp(\tau t/(\tau\tau))$. $\tau_{C1}$ was estimated using the exponential curve fit of experimental data (Figure 3).

## Systematic Instrument Error

Ideally, the instrument signal should show a zero base line when no samples are used. The instrument shows that, after an initial decrease, the dV signal increases with temperature.

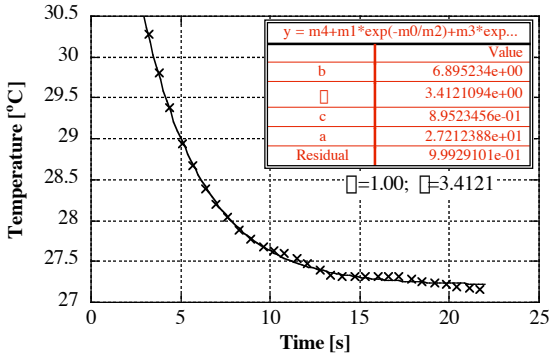


Figure 3. Estimation of conduction time constant, $\tau_{C1}$, using exponential curve fit of experimental data after the heated sample has been removed from the plate.

The same overall curve variation was observed when no pans were used and when platinum pans were used (Figure 4). This fact indicates that there are some intrinsic differences between the sample and reference side that cause a signal difference between the two sides of the instrument. This effect is now referred to as instrument asymmetry.

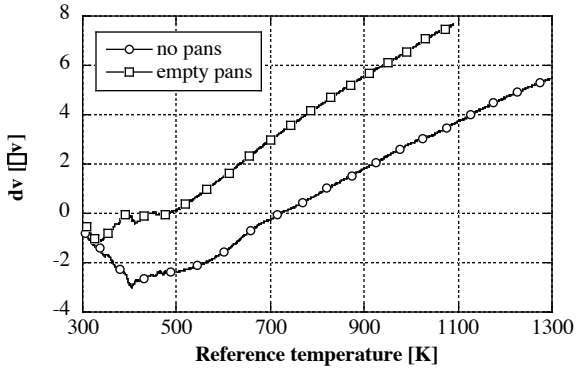


Figure 4. Signal difference between sample side and reference sides for no pan and empty pan cases showing a systematic instrument error.

Experiments indicate that the initial drop is due to (a) the mass difference between the sample side and reference side and (b) different time constants for the thermocouple assemblies on the sample and reference sides. By changing the position of the sensing unit inside the furnace, the systematic error may decrease but it cannot be removed. On the other hand, certain temperature distribution of the furnace walls is expected as well as a non-homogeneous temperature distribution within the DSC instrument such that the sample and reference plates are not at the same temperature. These geometric effects cannot be considered through simple conduction and radiation mechanisms between instrument parts. These geometric asymmetries must be modeled based on the actual curve variation of the systematic error.

## Numerical Simulation Results

A comprehensive DSC model was formulated in previous sections (see Table I). Since the model includes all the heat transfer interactions between different components of the DSC sensing unit it has a relatively large number of parameters. In this section, numerical simulation results are presented for several simplified models that were obtained by excluding some features of the detailed model. The computational results were compared against experimental data for empty containers, i.e. without sample and reference materials, and for pure aluminum in order to assess which are the most critical model features in order to qualitatively reproduce all the typical features of a DSC signal. Initially, experiments were

performed at heating rates of 20 $^{o}$C/min from room temperature until the set point reached a temperature of 1073K following by cooling with -20 $^{o}$C/min.

The several cases considered are identified in Table V. For each case, the parameters were varied such that a good agreement with experimental results was attained for a temperature domain as large as possible. The information on conduction parameters and relative range between radiation parameters presented in previous sections was used to limit the choice of parameters and their variation range. The representative parameters for each case were shown in Table VI. A variable considered for comparison was either the ratio between the reference plate temperature and set point temperature, *Tr/Tp*, or the difference between the sample plate temperature and reference plate temperature, *Ts-Tr*.

Table V. Cases considered for numerical simulations.

| Case id | Features of the DSC Model | | | |
|---|---|---|---|---|
| | Furnace-set point lag | Alumina Disk | Stem Heat loss | Radiation between containers |
| 1 | - | - | - | - |
| 2 | Y | - | - | - |
| 3 | Y | - | - | - |
| 4 | Y | Y | - | - |
| 5 | Y | Y | - | - |
| 6 | Y | Y | Y | - |
| 7 | Y | Y | Y | Y |

Table VI. Time constants [s] for cases considered for numerical simulations.

| Case id | Radiation Parameters | | | | | | | Furnace | Stem parameters | |
|---|---|---|---|---|---|---|---|---|---|---|
| | $\tau_{R1}$* | $\tau_{R2}$ | $\tau_{R3}$ | $\tau_{R4}$ | $\tau_{R5}$ | $\tau_{R6}$ | $\tau_{R8}$ | $\tau_{CF}$ | $\tau_{C7}$ | $\tau_{R7}$ |
| 1 | 650 | 3000 | 1500 | - | - | - | | - | - | - |
| 2 | 650 | 1000 | 1000 | - | - | - | | 40 | - | - |
| 3 | 650 | 2000 | 2000 | - | - | - | | 40 | - | - |
| 4 | 650 | 1000 | 680 | 220 | 200 | 6300 | | 40 | - | - |
| 5 | 650 | 1000 | 680 | 20 | 200 | 6300 | | 40 | - | - |
| 6 | 650 | 1000 | 680 | 220 | 200 | 6300 | | 40 | 2000 | 30000 |
| 7 | 650 | 1000 | 680 | 220 | 200 | 6300 | 4000 | 40 | 2000 | 30000 |

*$\tau_{R1}$ is not important to $T_R$ results. The following conduction parameters were considered $\tau_{C1}=\tau_{C2}=3.3$, $\tau_{C3}=\tau_{C4}=0.01$, $\tau_{C5}=1$, $\tau_{C6}=10$ s.

For the first case, a good agreement between numerical and computational results can be attained only in the low temperature domain (Figure 5 a). Including the furnace-set point lag feature was found to yield more realistic variation in the reference temperature (Figure 5 b). It was found that $\tau_{CF}$ governs the difference between Tr/Tp at cooling and heating. A value for $\tau_{CF}$ of 40 s was found to be the most appropriate. In Figure 5b, results were presented for the two extreme values of $\tau_{R2}$. For case 3, parameter $\tau_{R3}$ had to be varied accordingly in order to improve the agreement. At low values of $\tau_{R2}$ and $\tau_{R3}$, i.e., case 2, excellent agreement is observed again for low temperature domain. In order to improve the agreement at high temperatures, higher values of $\tau_{R2}$ and $\tau_{R3}$ are required, i.e., case 3. However, the numerical results have an unacceptable deviation from the experimental results at intermediate temperature ranges, i.e., between 360-550K. For the results presented in Figure 5, the alumina disk component was excluded. When the alumina disk was included in the model, the agreement with experimental results was improved at those temperature ranges where the previous model, represented by case 3, lacked a good agreement (Figure 6a).

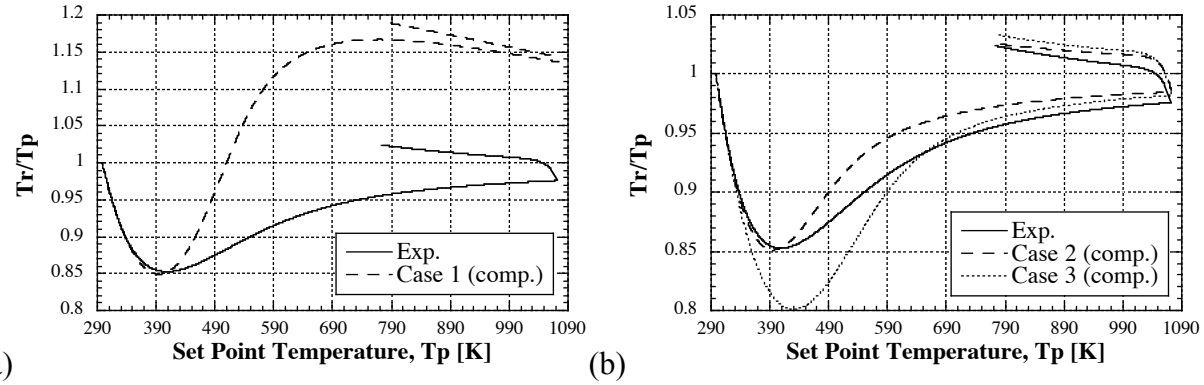


Figure 5. Ratio between the reference plate temperature and set point temperature for (a) case 1 and (b) cases 2 and 3 (Table VI).

However, a good agreement for the variation of *Tr/Tp* cannot be obtained by this model at temperatures above 800K, during both the heating and cooling domains. This effect is illustrated by case 5. In case 5, model parameters were varied such that a good agreement was obtained at high temperatures during heating. As seen in case 3, a poor agreement is again recorded at intermediate temperatures. Moreover, the *Tr/Tp* curve has moved upwards at cooling, increasing the error of the numerical simulation results. Next, the heat transfer losses through the stem that supports the alumina disk were considered. We thought that including this effect could be important since the mounting end of the stem is held at constant temperature of about 340K using additional water cooling. A good agreement at all temperature ranges was obtained when this feature was considered (Figure 6b).

In order to test the proposed methodology, the experiments at other heating and cooling rates were considered (Figure 7a). The model parameters were those considered for case 6. These additional subcase simulations were labeled with the corresponding heating and cooling rates. In all the subcases considered, the heating rates were 20 $^{o}$C/min until the set point reached 873K. The subcases were labeled with M/N, where M=20 represents the first heating rate and N the corresponding second heating rate in $^{o}$C/min. Cooling was performed with the same rate as that of the last heating segment. Only the high temperature domain is shown in Figure 7a. The agreement on heating for all heating rates is excellent. This excellent agreement at variable heating rates validates the proposed model. Right after the heating/cooling transition, the computed ratios *Tr/Tp* are larger than the experimental ones and follow quite well the experimental results at cooling. At cooling, the slope of the *Tr/Tp* curve is smaller than those corresponding to experimental results.

The next step in the analysis of the DSC signal is to investigate relevant model parameters to the phase transition. DSC experiments were conducted for a pure aluminum sample (mass 0.01714g). A sapphire reference material of 0.04212 g was placed in the reference container. A small effect of the phase change is seen on the reference side (Figure 7b). When the radiation between the two containers is not included, the computed *Tr/Tp* increases with the same rate as that before the phase change. The characteristic behavior of *Tr/Tp* during the phase change can be accurately reproduced when (a) $\tau_{C1}$=3.3 s and the radiation between the two containers is included, or (b) $\tau_{C1}$=0.33 s and the radiation between the two containers is excluded.

For *Ts-Tr*, experimental results are compared against numerical simulation results for empty containers (Figure 8a). The computed values are lower at heating and higher at cooling than the experimental data. This result indicates that conduction and radiation parameters alone cannot account for the asymmetry seen in the experiments and an asymmetry submodel has to be developed. Experiments were conducted for pure aluminum.

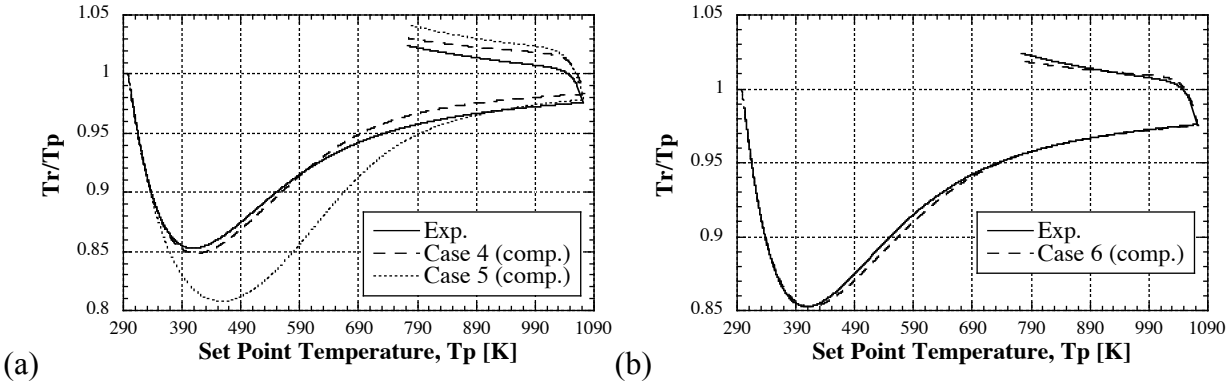


Figure 6. Ratio between the reference plate temperature and set point temperature for (a) cases 4 and 5, and (b) case 6 (Table VI).

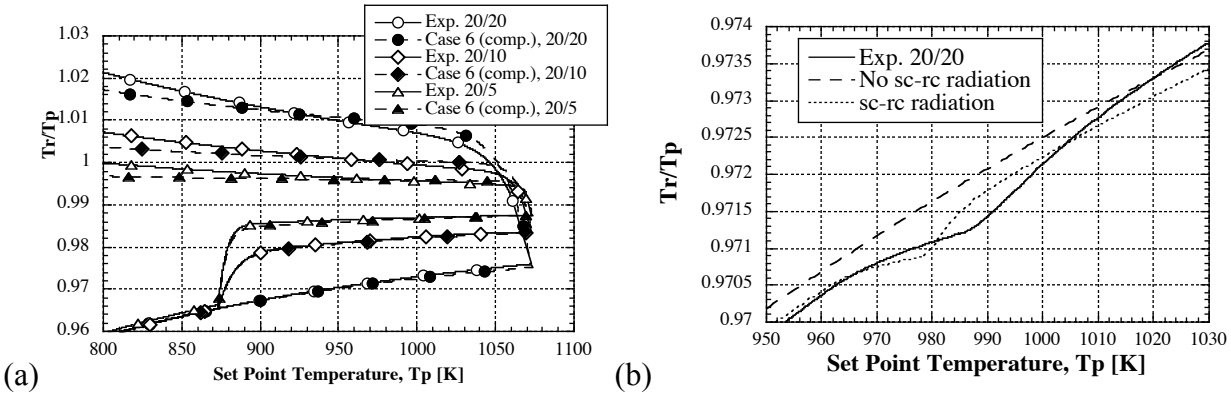


Figure 7. *Tr/Tp* results for (a) variable heating and cooling rates of empty pan (case 6) (b) temperature lag on the *reference* side for a pure aluminum sample (cases 6 and 7, Table VI).

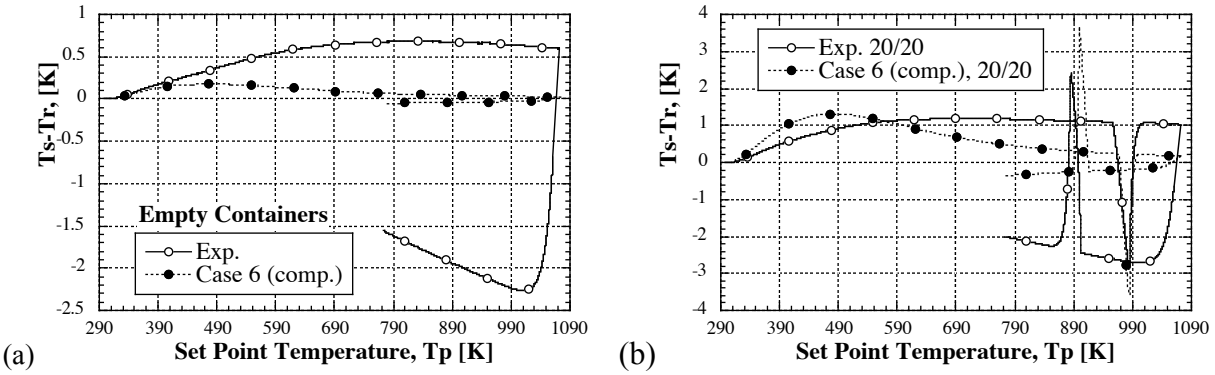


Figure 8. Temperature difference between the sample plate and reference plate for (a) empty containers, and (b) pure aluminum sample.

Numerical simulations were performed for case 6 by including the sample and reference into the analysis. The results were presented for the temperature difference *Ts-Tr* in Figure 8b. The abrupt variations in the *Ts-Tr,* which are due to the phase transformations, can be qualitatively reproduced by the proposed model. The computed values *Ts-Tr* are lower at heating and higher at cooling than the experimental data.

## Conclusions

For the Netzsch DSC 404C instrument with high accuracy heat capacity sensor, a mathematical model was developed by assuming that each component is isothermal and that the heat transfer

among components occurs by conduction and radiation. Model parameters are effective conduction time constants and radiation time constants.

Several model cases have been investigated to assess the effect of heat transfer interactions considered. New features that have not been considered in previous DSC models were include in the present study. These new features include (a) considering the sensor platform, (b) accounting for the heat loss through the stem, (c) considering the lag between furnace temperature and set point temperature. Comparisons with experimental results show that temperature lags in heat flux DSC instruments can be determined by conducting a heat transfer analysis based on a comprehensive model. The proposed mathematical model yields accurate results over a wide temperature range, during heating and cooling regimes. Instrument asymmetry is documented. These asymmetry effects cannot be considered through simple conduction and radiation mechanisms between instrument parts.

## Acknowledgments

This work was sponsored by the U.S. Department of Energy, Assistant Secretary for Energy Efficiency and Renewable Energy, Industrial Technologies Program, Industrial Materials for the Future (IMF), under contract DE-AC05-00OR22725 with UT-Battelle, LLC and Office of FreedomCAR and Vehicle Technologies, as part of the High Temperature Materials Laboratory User Program, Oak Ridge National Laboratory.

## References

Gray, A. P. in *Analytical Calorimetry*, ed. R. S. Porter and J. F. Johnson, Plenum Press, New York, 1968, pp. 209.

Jeng, S. and Chen, S., The Solidification Characteristics of 6061 and A356 Aluminum Alloys and Their Ceramic Particle-Reinforced Composites, Acta Mater., Vol. 45, No. 12, pp. 4887-4899, 1997.

Wolfinger, M.G., Rath, J., Krammer, G., Barontini, F., and Cozzani, V., Influence of the Emissivity of the Sample on Differential Scanning Calorimetry Measurements, Thermochimica Acta 372 (2001) pp. 11-18.

Dong, H. B. and Hunt, J. D., A Numerical Model of a Two-Pan Heat Flux DSC, Journal of thermal analysis and Calorimetry, Vol. 64 (2001) pp. 167-176.

Speyer, R. F., Deconvolution of Superimposed DTA/DSC Peaks Using the Simplex Algorithm, J. Mater. Res., Vol. 8, No. 3, 1993.

Kempen, A.T.W., Sommer, F., and Mittemeijer, E.J., Calibration and Desmearing of a Differential Thermal Analysis Measurement Signal Upon Heating and Cooling, Thermochimica Acta 383 (2002) pp. 21-30.

Danley, Robert L., New Heat Flux DSC Measurement Technique, Thermochimica Acta 395 (2003) pp. 201-208.

Boettinger, W.J. and U. R. Kattner, On Differential Thermal Analyzer Curves for the Melting and Freezing of Alloys, Metallurgical and Materials Transaction A, Vol. 33A, June 2002, pp. 1779-1794.